Static and dynamic magnetic properties of spherical magnetite nanoparticles

G. F. Goya,[a] T. S. Berquó, and F. C. Fonseca
Instituto de Física, Universidade de São Paulo, CP 66318, 05315-970, São Paulo, SP, Brazil

M. P. Morales
Instituto de Ciencia de Materiales de Madrid, CSIC, Cantoblanco, 28049-Madrid, Spain

(Received 28 March 2003; accepted 23 June 2003)

We present a detailed study of static and dynamic magnetic behavior of Fe_3O_4 nanoparticles with average particle sizes $\langle d \rangle$ ranging from 5 to 150 nm. Bulk-like properties such as saturation magnetization, hyperfine parameters, coercive field, and Verwey transition are observed in 150 nm particles. For decreasing particle size, the Verwey temperature, T_V, shifts down to ~20 K for $\langle d \rangle = 50$ nm and is no longer observable for smaller particles. The smallest particles ($\langle d \rangle = 5$ nm) display superparamagnetic behavior at room temperature, with transition to a blocked state at $T_B \sim 45$ K, which depends on the applied field. The existence of surface spin disorder can be inferred from the decrease of saturation magnetization M_S at low temperatures, as the average particle size is reduced. This disordered surface did not show effects of exchange coupling to the particle core, as observed from hysteresis loops after field cooling in a 7 T magnetic field. For particles with $\langle d \rangle = 5$ nm, dynamic ac susceptibility measurements show a thermally activated Arrhenius–Néel dependence of the blocking temperature with applied frequency. The interparticle interactions are found to influence the energy barriers yielding an enhancement of the estimated magnetic anisotropy. From the calculus of the magnetic anisotropy, it is inferred that there is no structural transition from cubic to triclinic symmetry for $\langle d \rangle = 5$ nm, in agreement with the absence of the Verwey transition. A value $K_1 = 4.68 \times 10^5$ erg/cm^3 is obtained for the magnetocrystalline anisotropy constant of the cubic phase. © *2003 American Institute of Physics.*
[DOI: 10.1063/1.1599959]

I. INTRODUCTION

Nanosized magnetic structures are currently key materials for advancements in electronics,[1] optoelectronics,[2] magnetic storage,[3] and many bioinspired applications.[4–6] What is usually termed ''nanostructured systems'' comprises those materials whose properties are determined by entities (particles, crystallites, or clusters) with characteristic lengths between 1 and 100 nm in at least two dimensions. If the grain or domain size becomes comparable or smaller to the characteristic length scale of the interaction processes controlling a particular property, different effects and unusual chemical and physical properties can be expected that are highly attractive in a number of technical applications.[7–9] In recent times, large advancements have been achieved related to the synthesis and characterization of well-defined, discrete magnetic nanoparticles for both fundamental and technological purposes. However, precise knowledge of the relationships between particle shape and size distribution, surface structure, and the resulting magnetic properties of magnetic nanoparticles is still lacking. This remains true even for particles composed of ''simple'' pure materials such as Fe, Co, or Ni, whose bulk properties are well understood.[10]

Magnetite Fe_3O_4 has recently attracted attention because bulk Fe_3O_4 has a high Curie temperature ($T_C \sim 850$ K) and nearly full spin polarization at room temperature, both properties of great potential for applications in giant magnetoelectronic and spin-valve devices based on magnetite films. In spite of the fact that magnetite is perhaps the oldest magnetic material known, some aspects on the basic mechanisms related to the Verwey transition are still being discussed, especially in nanosized systems.[11,12] An additional issue to be solved for potential applications is that the magnetic properties of magnetite-based nanostructured systems (particles or films) strongly depend on the synthesis route,[13–15] as well as on the nonmagnetic matrix (or substrate) chosen. Moreover, for a given synthesis technique the final magnetic properties seem to depend heavily on tiny changes in the local structure like antiphase boundaries (APB), oxygen deficiency, and local ionic disorder.[16–18]

Above the Verwey temperature, $T_V \sim 120$ K, magnetite has a cubic spinel structure (space group $Fd3m$), with lattice parameter $a_0 \sim 8.397$ Å and the O atoms arranged in a face-centered-cubic (fcc) lattice. The lattice can accommodate Fe^{3+} on the tetrahedral site (A) and Fe^{3+} and Fe^{2+} on the octahedral site (B) in antiparallel arrangement, yielding ferrimagnetic order below T_C. Bulk magnetite has cubic magnetic anisotropy, with the $\langle 1\ 1\ 1 \rangle$ and $\langle 1\ 0\ 0 \rangle$ directions being the easy and hard axes of magnetization, respectively. At room temperature (RT), the first-order magnetocrystalline anisotropy constant has a negative value ($K_1 = -1.35 \times 10^5$ erg/cm^3) that changes sign at low temperature, passing through an isotropic point at a temperature few degrees

[a]Electronic mail: goya@macbeth.if.usp.br

above the Verwey transition.[19] On cooling below T_V, the change from cubic to triclinic structure yields a change to uniaxial anisotropy with $\langle 0\ 0\ 1\rangle$ easy axis.[20]

Since the magnetic hardness of single-domain particles results from the concurrent effects of shape and crystal anisotropies, there is an obvious need for separating these effects to study each of them. As the magnetocrystalline anisotropy is associated with each material and cannot be eliminated, we have chosen a simple way for disentangling these effects by making spherical particles to eliminate the shape anisotropy. In this work, we present a detailed structural and magnetic characterization of spherical Fe_3O_4 nanoparticles with different mean sizes from 5 to 150 nm, aiming to study the relation between structural and magnetic properties in the blocked state as well as in the superparamagnetic (SPM) regime.

II. EXPERIMENTAL PROCEDURE

Four magnetite (Fe_3O_4) samples have been prepared by different routes and named according to their mean particle size (in nanometers): samples M150, M50, M10, and M5. Sample M150 was prepared by first precipitating hematite particles by forced hydrolysis of a 0.02 M $FeCl_3$ solution at 100 °C during 2 days[21] and further reduction under 1 atm of hydrogen at 360 °C during 3.5 h. Sample M50 was obtained after heating at 90 °C a solution of 0.1 M KOH and 0.05 M $FeSO_4$ during 24 h, in the presence of 0.2 M of KNO_3.[22] Sample M50 was washed with HCl and later with water. Sample M10 was prepared by adding 50 ml of an aqueous solution (0.33 M $FeCl_2$ and 0.66 M $FeCl_3$) to 450 ml of 1 M ammonium hydroxide under constant stirring at room temperature.[23] During preparation of both M10 and M50 samples, N_2 gas was flowed previously through the base solution and the formed black precipitate was washed and dried at 40 °C during 2 h in air. Sample M10 was washed with water. Smaller particles of around 5 nm were obtained following the Lee *et al.* method.[24] The iron salt mixture, Fe(II) and Fe(III), was added to 1 M K(OH) solution with 1 wt % of polyvinylalcohol (PVA) at room temperature.

X-ray diffraction (XRD) measurements were performed using a Philips 1710 powder diffractometer using Cu $K\alpha$ radiation in the 2θ range from 5° to 70°. Transmission electron microscopy (TEM) images were taken in a high-resolution 200 keV JEOL-2000 FXII microscope, in order to analyze the structure and morphology of the magnetic powders. Mössbauer spectroscopy (MS) measurements were performed with a conventional constant-acceleration spectrometer in transmission geometry with a source of about 50 mCi ^{57}Co in a Rh matrix between 78 and 296 K. Hyperfine parameters such as the distribution of hyperfine magnetic field, isomer shift, and quadrupole shift have been determined by the NORMOS program, and α-Fe at 296 K was used to calibrate isomer shifts and velocity scale. Room temperature M vs H cycles were performed in a vibrating sample magnetometer using an electromagnet to produce fields up to 2 T. Static and dynamic magnetic measurements as a function of frequency and temperature were performed in a commercial superconducting quantum interference device (SQUID) magnetometer (Quantum Design). Zero-field-cooled (ZFC) and field-cooled (FC) curves were taken between 5 and 400 K, for different values of cooling field H_{FC} ($10\ \text{Oe} < H < 70\ \text{kOe}$). Data were obtained by first cooling the sample from room temperature in zero applied field (ZFC process) to the basal temperature (5 K). Then, a field was applied and the variation of magnetization was measured with increasing temperature up to $T = 400$ K. After the last point was measured, the sample was cooled again to the basal temperature keeping the same field (FC process); then, the M vs T data were measured for increasing temperatures.

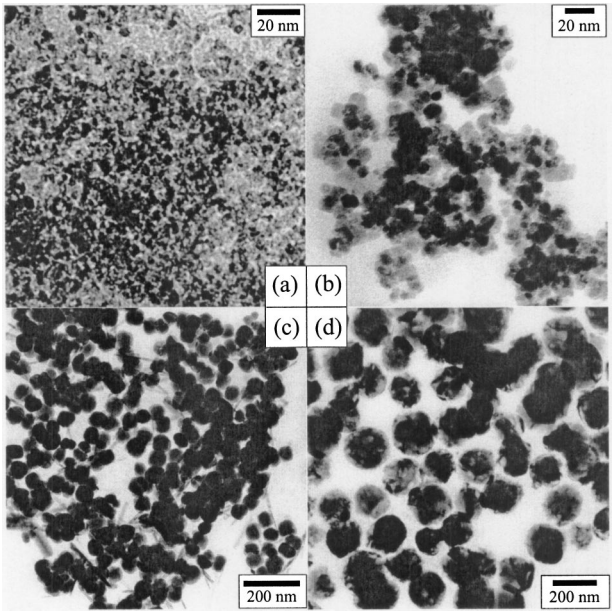

FIG. 1. TEM pictures for samples M5 (a), M10(b), M50 (c), and M150 (d).

III. EXPERIMENTAL RESULTS

Analysis of TEM images (Fig. 1) showed that the resulting samples consist of homogeneous particles with nearly spherical shape, increasing the size from M5 to M150 samples. The resulting average size estimated from these images are displayed in Table I. The x-ray diffractograms for the four samples shown in Fig. 2 could be indexed with the Fe_3O_4 single phase, except for the M50 sample where small peaks corresponding to the main reflections of goethite were observed. It can be noticed that the lines broaden steadily from the M150 to M5 sample as a result of the decrease in the average particle size, in agreement with TEM data. We have estimated the average grain size $\langle d\rangle$ from the main reflections of each diffractogram, by using the Scherrer formula and without considering possible contributions of crystal stress to the observed linewidth. It can be seen from Table I that the agreement between TEM and XRD data is very good, giving support to the following discussion on the magnetic properties of these particles.

A. Mössbauer study

The Mössbauer spectra of Fe_3O_4 particles with different sizes, at 296 and 78 K, are shown in Figs. 3 and 4, respectively. A first, general feature that can be observed at RT is

TABLE I. Average particle diameters $\langle d \rangle$ extracted from TEM and x-ray data, saturation magnetization M_S, coercive field H_C, remanence M_R, and the ratio $R = M_R/M_S$ for Fe_3O_4 samples measured at 5 and 300 K.

Sample	Particle size (TEM) (nm)	Crystal size (x-ray) (nm)	Temp (K)	H_C (Oe)	M_S (emu/g)	M_R (emu/g)	M_R/M_S
M5	4	4.3	5	294(10)	56.1(2)	10.1(8)	0.15
			300	12(7)	31.8(2)	0	0
M10	11.5	~10	5	202(10)	77.5(2)	12.7(8)	0.16
			300	34(7)	60.1(2)	3.9(2)	0.016
M50	47.7	55	5	211(10)	77.8(2)	16.3(8)	0.21
			300	156(7)	65.4(2)	16.4(2)	0.25
M150	~150	~150	5	736(10)	88.5(2)	32.1(8)	0.36
			300	323(7)	75.6(2)	18.9(2)	0.25

the gradual passage from bulk-like to SPM behavior, as the average particle size decreases. For sample M150, the room temperature spectrum was fitted using two magnetic components of hyperfine fields $B_{hyp} = 49.5$ and 46.0 T, corresponding to Fe^{3+} ions at sites A and (Fe^{2+} Fe^{3+}) ions at site B, respectively (see Table II), with nearly null quadrupole splitting (QS) and intensity ratio $B{:}A \sim 1{:}1$. These well-known features of MS are related to the electron transfer process (electron hopping) between Fe^{2+} and Fe^{3+} ions on the octahedral B site taking place for $T > 115-120$ K (Verwey transition). The absence of SPM signal (doublet) in the MS shows that these particles have a multidomain structure, in agreement with the theoretical estimation for *maximum* linear dimensions of single-domain particles of ~128 nm.[25,26]

As particle size decreases, both hyperfine fields merge into a single sextet (sample M50), and for sample M10 the thermal relaxation effects are clearly observed (Fig. 3). Additionally, sample M50 showed a small component from goethite ($B_{hyp} = 37.7$ T), amounting to a ~3% of the total spectral area, in agreement with XRD data. Sample M5 displays only a central doublet corresponding to a full superparamagnetic state.

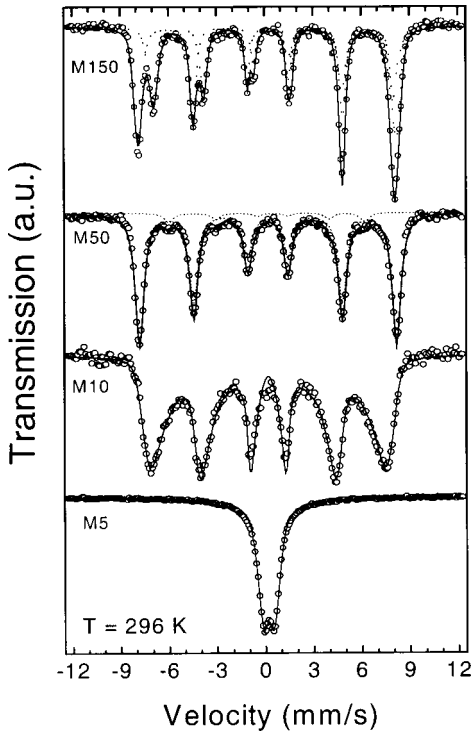

FIG. 3. Mössbauer spectra (open circles) recorded at 296 K for the Fe_3O_4 samples. The solid lines are the best fit to experimental data, and dotted lines represent each component of the total fit.

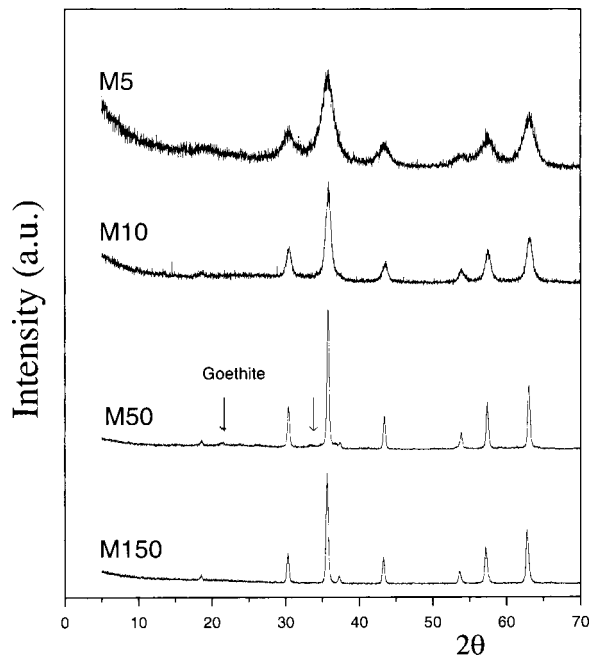

FIG. 2. X-ray diffraction patterns of the Fe_3O_4 samples with different average particle sizes.

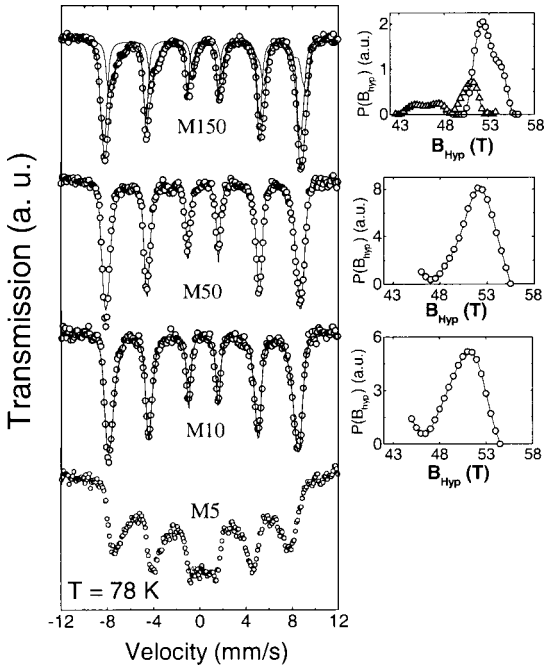

FIG. 4. Left panel: Mössbauer spectra (open circles) recorded at 78 K for the Fe_3O_4 samples. Solid lines are the best fits using hyperfine field distributions $P(B_{hyp})$ shown on the right panel.

TABLE II. Hyperfine parameters extracted from Mössbauer spectra at $T=296$ K: hyperfine field (B_{hyp}), quadrupolar splitting (QS), isomer shift (IS), and spectral area (I) for samples M5, M10, M50, and M150.

T (K)	Sample	Site	B_{hyp} (T)	QS (mm/s)	IS (mm/s)	I (%)
296	**M5**		-	0.60(1)	0.22(1)	100(3)
	M10		46.0	0.00(1)	0.21(1)	100(3)
	M50		50.0	0.00(1)	0.22(1)	100(3)
	M150	*A*	49.5	0.05(1)	0.20(1)	57(3)
		B	46.0	0.02(1)	0.64(1)	43(3)

At $T=78$ K (i.e., below the Verwey transition) the spectrum of sample M150 shows the change of lattice symmetry to the low-temperature (triclinic) phase.[20,27] We attempted to fit the spectrum with two distributions of hyperfine fields, corresponding to Fe^{3+} ions at *A* sites and to Fe^{2+} and Fe^{3+} at *B* sites. The resulting distributions are shown on the right side of Fig. 4. There is not general agreement about the type of fit that best reflects the properties of the magnetite phase at low temperatures, and different authors have proposed from two to more than five magnetic components for $T<T_V$.[28,29] However, there are several common features observed in almost all low-T spectra reported, such as the increase of B_{hyp} and the nearly zero QS values. For samples M50 and M10, the spectra at 78 K showed that the thermal fluctuations observed at room temperature are no longer present. Moreover, using a second site distribution did not improve the fits, therefore, these spectra were fitted using a single magnetic sextet. The resulting distribution profiles showed a maximum centered at $B_{hyp}\sim 52.3$ and 51.2 T for M50 and M10, respectively. For sample M5 thermal relaxation effects are still dominant at this temperature, in agreement with the blocking temperature of ~45 K observed from magnetization data (see below).

B. Magnetization study

To better understand the magnetic properties of these systems we performed magnetization measurements as a function of temperature and applied fields. The ZFC/FC curves (Fig. 5) of the M150 sample show clearly that the Verwey transition is still present, although at a lower temperature ($T_V=98(1)$ K). Sample M50 still shows a kink at ~16 K, probably related to the Verwey transition, which is shifted to a lower temperature due to size effects. Additionally, a broad maximum is observed in the ZFC sample centered at $T_B\sim 300$ K, suggesting a blocking process of large particles. For M10 and M5 samples the maximum at T_B shifts to 107(1) and 45(1) K, respectively, and the Verwey transition is no longer observable.

The dependence of the high-field magnetization with temperature is shown in Fig. 6. Since the magnetization of the sample at 70 kOe is only ~5% below the saturation value M_S extracted from extrapolation to infinite field, we can consider that $M_S(T)=M(T,H=70\ \text{kOe})$. It can be seen from Fig. 6 that $M_S(T)$ steadily decreases with increasing T, and this thermal decrease could be fitted by the Bloch law

$$M_S(T)=M_S(0)[1-B_0T^{3/2}],$$

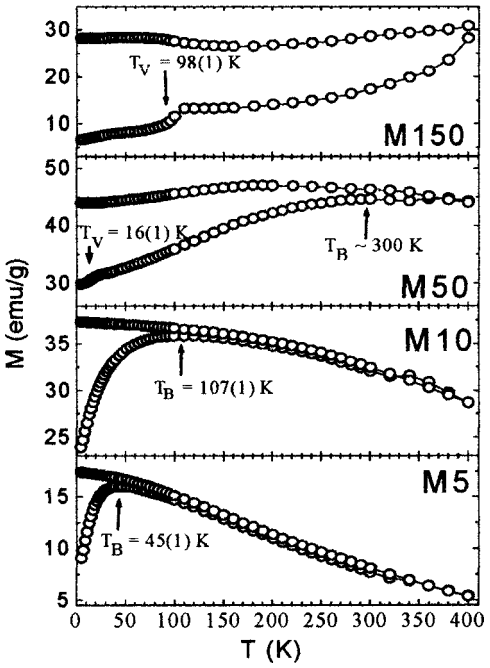

FIG. 5. Zero-field-cooled (ZFC) and field-cooled (FC) curves for samples of different particle sizes, taken with $H_{FC}=500$ G.

where $M_S(0)$ is the saturation magnetization at zero temperature. This is in contrast to previous results reported on a system of magnetite particles suspended in a ferrofluid,[30] where a T^2 dependence (slightly modified by a T-dependent prefactor) was proposed. The inset of Fig. 6 clearly shows that the linear relation between $[M_S-M_S(T)]/M_S$ vs $T^{3/2}$ is followed along the whole experimental temperature range ($5\ \text{K}\leqslant T\leqslant 350$ K). Although theoretical calculations[31] have predicted a thermal dependence of the form T^{α} with $3/2<\alpha<3$ for small ferromagnetic clusters, many nanostructured systems such as α-Fe particles in the SiO_2 matrix[32] and γ-Fe_2O_3 nanoparticles[33] have provided experimental evidence for the $T^{3/2}$ dependence at least up to room temperature. For the present magnetite nanoparticles, the prefactor $B_0=3.3\times10^{-5}\ \text{K}^{-3/2}$ obtained from the fitting procedure is

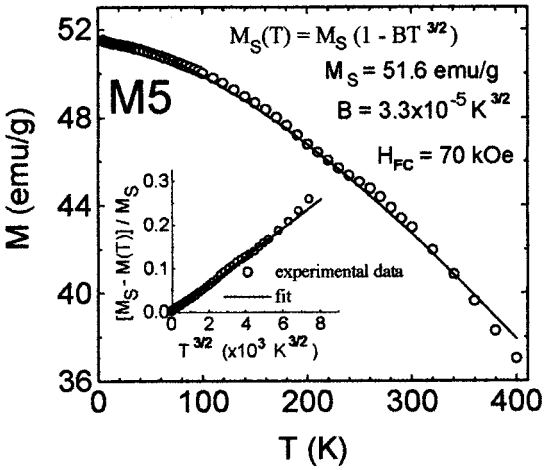

FIG. 6. Magnetization vs temperature for M5 sample taken at $H=70$ kOe (open circles). The solid line is the fit using the Bloch law. Inset: graph $M(T)$ vs $T^{3/2}$ to show the linear relationship up to ~350 K.

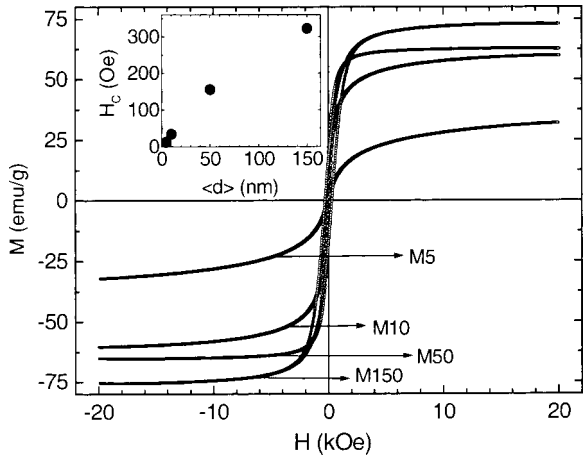

FIG. 7. Magnetization hysteresis curves measured at 296 K for the Fe_3O_4 samples.

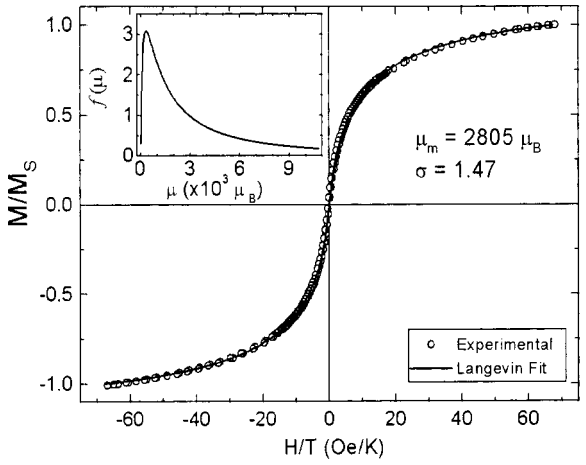

FIG. 8. Superparamagnetic contribution M^{sp} of sample M5 at $T=296$ K. The solid line is the fitted curve obtained from Eqs. (1) and (2). Inset: resulting distribution function with $D_0=5.0$ nm and $\sigma=1.4$.

similar to the 2.8×10^{-5} $K^{-3/2}$ observed for γ-Fe_2O_3 particles.[33] Furthermore, the similarity of B_0 values in Fe_3O_4 and γ-Fe_2O_3 nanoparticles can be understood from (a) their common cubic crystal structure (space group O_h^7-$Fd3m$); (b) their close lattice parameters a (~8.35–8.39 Å); and (c) their similar ordering temperatures (~600 °C) that involve similar exchange integral values J.[34] As pointed out by Martínez *et al.*,[33] the $T^{3/2}$ dependence indicates the existence of spin-wave excitations in these nanometric domains of few-nanometer size. Using a very simplified landscape for the thermal excitation of the magnons at low temperatures, the prefactor B of the Bloch law can be expressed as $B_0^{-1}\sim D=2a^2JS$, where D is the spin-wave stiffness constant, and S is the spin of magnetic ions. From this relationship we extracted an average value of $J/k_B=23$ K, which is of the same order of magnitude that the exchange constant J_{AB} between A and B sublattices in bulk magnetite.[34]

Hysteresis loops performed at room temperature (Fig. 7) show that the coercivity decreases with decreasing particle size, attaining zero value for the M5 sample, in agreement with the SPM behavior for a $\langle d\rangle=5$ nm particle size. It is also observed that samples M150 and M50 are already saturated at $H=20$ kOe, whereas samples M10 and M5 show still slightly increasing magnetic moment. For the latter two samples, the M_S values (Table I) were obtained from the relationship $M=M_S\ (1-\beta/H)$, where β is a field-independent parameter, after extrapolating to infinite field. The results obtained differ from the $M(H=20\ \text{kOe})$ values by 3% and 11% for the M10 and M5 samples, respectively.

In the SPM regime, the magnetization $M^{sp}(H)$ plotted against H/T results in a universal curve, described by the relation $M^{sp}=N\mu L(x)$, where N is the number of particles of magnetic moment μ, and $L(x)$ is the Langevin function of argument $x=\mu H/kT$, i.e., the ratio of magnetic to thermal energy. To take into account the effects of size dispersion always present in any real system, the magnetization of SPM grains in a magnetic field H is better described as a weighted sum of Langevin functions

$$M^{sp}=M_S^{bulk}\int_0^\infty L\left(\frac{\mu H}{kT}\right)f(\mu)d\mu, \tag{1}$$

where $f(\mu)$ is a log–normal distribution

$$f(\mu)=\frac{1}{\sqrt{2\pi}\,\sigma\mu}\exp\left(-\frac{(\ln\mu/\mu_0)^2}{2\sigma^2}\right) \tag{2}$$

of magnetic moments μ. In Eq. (2), σ is the distribution width and μ_0 is the median of the distribution related to the mean magnetic moment μ_m by $\mu_m=\mu_0\exp(\sigma^2/2)$. The distribution function satisfies the normalization condition

$$M_S=\int_0^\infty f(\mu)d\mu.$$

In order to obtain the magnetic moment distribution for the M5 sample, we have fitted the $M(H)$ data using Eqs. (1) and (2), which contains two free parameters (μ_0 and σ). The result is shown in Fig. 8. To relate the moment distribution to the particle size distribution we have used the saturation magnetization value $M_S=398.7$ emu/cm^3, as extracted from Table I. Also, based on the TEM data, we have presumed spherical geometry for particles, i.e., $V=\pi D^3/6$ where D is the particle diameter. With these assumptions we obtained the values $\mu_0=2805\ \mu_B$ and $D_0=5.0$ nm, the latter being in excellent agreement with estimations from TEM and x-ray diffraction. Fitting the $M(H)$ data with a simple Langevin function yielded values $\mu=6599\ \mu_B$ and $D=6.7$ nm, which are slightly larger than the values from the log-normal distribution $f(\mu)$ of magnetic moments. The different values reflect mainly the difference between median (μ_0) and mean (μ_m) values of the magnetic moment distribution, related to the distribution width $\sigma^2=2\ln(\mu_m/\mu_0)$.

In order to see possible effects of exchange coupling between core and surface of the particles, hysteresis loops were also measured at 5 K after field cooled in a 7 T field. As shown in Fig. 9, the cycles are symmetric within experimental error (i.e., no exchange bias can be observed), indicating the lack of exchange coupling between particle surface and core. At low temperatures, it is observed that the saturation magnetization decreases for smaller particles, indicating increasing spin disorder effects at the particle surface, yielding a smaller net magnetic moment.

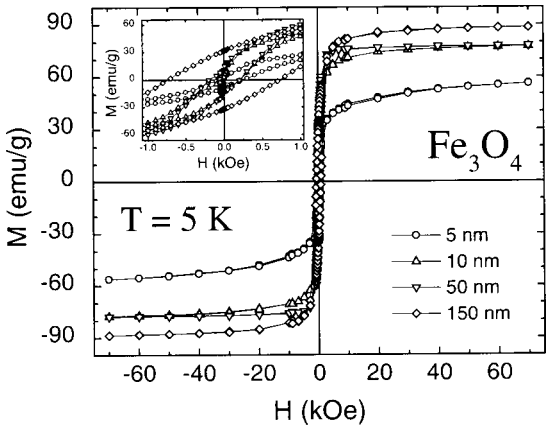

FIG. 9. Magnetization hysteresis curves measured at 5 K for the Fe_3O_4 samples in field-cooling mode with $H_{FC}=7$ T. Inset: amplification of the low-field region showing the symmetry of the loops.

C. Dynamic properties

Turning now to the dynamics of the magnetic particle systems, Fig. 10 displays the temperature dependence of $\chi'(T)$ and $\chi''(T)$ of the smallest particles (sample M5) for different frequencies f ranging from 20 mHz to 1 kHz. The data for both components $\chi'(T)$ and $\chi''(T)$ exhibit the expected behavior of SPM systems, i.e., the occurrence of a maximum at a temperature T_m for both $\chi'(T)$ and $\chi''(T)$ components, which shifts towards higher values with increasing frequency.[35] As a useful criterion for classifying the freezing/blocking process observed, we used the empirical parameter Φ, which represents the relative shift of the temperature T_m per decade of frequency. For the M5 sample, we obtain

$$\Phi = \frac{\Delta T_m}{T_m \Delta \log_{10}(f)} = 0.07,$$

where ΔT_m is the difference between T_m measured in the $\Delta \log_{10}(f)$ frequency interval. This value is close to the 0.10 value found for SPM systems, providing a model-independent classification of the thermally activated origin of

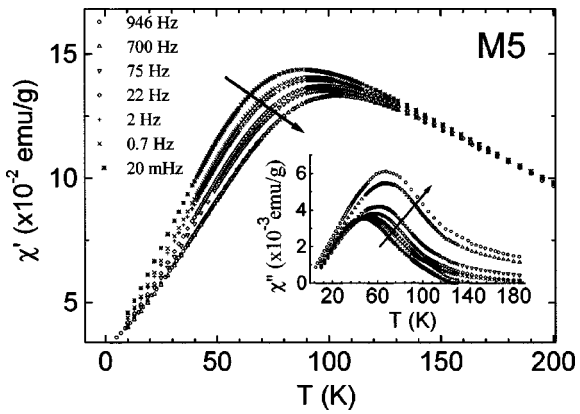

FIG. 10. Temperature dependence of the in-phase (real) component $\chi'(T)$ of the magnetic susceptibility for the M5 sample, at different excitation frequencies. Arrows indicate increasing frequencies. Inset: Out of phase (imaginary) component $\chi''(T)$. The data were taken with an external magnetic field $H=5$ Oe.

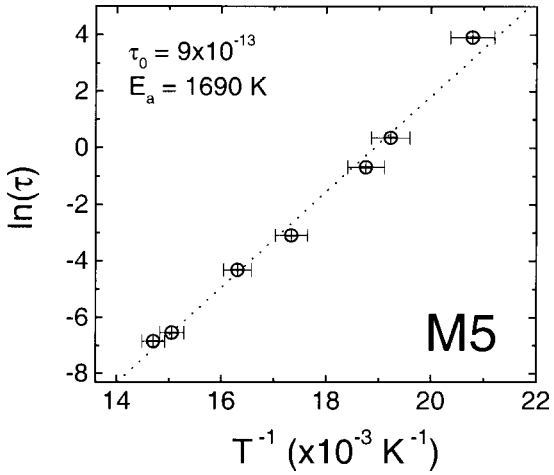

FIG. 11. Arrhenius plot of the relaxation time τ vs inverse blocking temperature T_B^{-1} obtained from the imaginary component $\chi''(T)$ as extracted from Fig. 9. Dotted line is the best fit using Eq. (3) with $\tau_0=9\times10^{-13}$ s and $E_a=1690$ K.

the observed transition. On the other side, it is known that smaller values of Φ usually result from spin-glass-like surface behavior or interparticle interactions.[35–37] The latter corresponds more likely to the present case, since our samples are nondiluted particulate systems.

The dynamic response of an ensemble of fine particles is determined by the measuring time τ_m (or frequency) of each experimental technique. As the reversion of the magnetic moment in a single-domain particle over the anisotropy energy barrier E_a is assisted by thermal phonons, the relaxation time τ exhibits an exponential dependence on temperature characterized by a Néel–Arrhenius law

$$\tau = \tau_0 \exp\left(\frac{E_a}{k_B T}\right), \tag{3}$$

where τ_0 is in the 10^{-9}–10^{-11} s range for SPM systems. In the absence of an external magnetic field, the energy barrier can be assumed to be proportional to the particle volume V, $E_a = K_{\text{eff}} V \sin^2\theta$, where K_{eff} is an effective magnetic anisotropy constant and θ is the angle between the magnetic moment of the particle and its easy magnetization axis.

The linear dependence of $\ln(f)$ vs $1/T_B$ observed in Fig. 11 indicates that the Néel–Arrhenius model correctly suits the behavior of the M5 sample. From the fitting of the experimental $T(f,H=0)$ data using Eq. (3) and the average particle radii from TEM data, we obtained the values of $K_{\text{eff}}=35.6\times10^5$ erg/cm^3 and $\tau_0=9\times10^{-13}$ s. The resulting effective anisotropy is an order of magnitude larger that the magnetocrystalline anisotropy (first-order) constant of bulk magnetite $K_1^{\text{bulk}}=1.35\times10^5$ erg/cm^3, and this enhancement observed in nanoparticles is customarily associated to surface effects.[10,38] However, as will be discussed later, for a spherical particle the contribution of the surface anisotropy should average to zero, and therefore no contribution can be expected from the surface in the present particles. It is worth to notice that, in addition to the contributions from the intrinsic particle anisotropy to E_a (such as shape, magnetocrystalline, or stress anisotropies), interparticle interactions (di-

polar or exchange) can also modify the energy barrier.[39] In a previous work on Fe_3O_4 particles of $d=5$ nm, diluted in a ferrofluid,[40] it was found that dipolar interactions are already noticeable for concentrations of ~2 vol % of magnetic particles. When comparing against our data on $\langle d\rangle=5$ nm particles, the larger blocking temperature at low fields observed in our sample further agrees with the presence of strong dipolar interactions due to the higher concentration of magnetic particles. Therefore, the value of K_{eff} obtained for the present nondiluted system clearly contains the effect of particle–particle interactions and must be taken with great caution.

IV. DISCUSSION

Recently, several works on nanometer-sized magnetite particles and films obtained by different techniques have found that the resulting materials may display large differences regarding their magnetic properties. These differences are attributed to changes in structural disorder,[41] creation of antiphase boundaries,[17] or the existence of a magnetically dead layer at particle surface.[42] However, other SQUID and magneto-optical Kerr effect measurements performed on magnetite films[43,44] showed that bulk-like behavior can be present for linear dimensions down to 10 nm.

The saturation magnetization values found in nanostructured materials are usually smaller than the corresponding bulk phases, provided that no changes in ionic configurations occur. Accordingly, experimental values for M_S in magnetite nanoparticles have been reported to span the 30–50 emu/g range, lower than the bulk magnetite value ~90 emu/g.[45] Many studies have been reported on the origin of the observed reduction in magnetization in fine magnetic particles. The first studies on the decrease in magnetization performed in γ-Fe_2O_3 by Coey[46] showed that this reduction is due to the existence of noncollinear spins at the surface, making the same mechanism appealing for Fe_3O_4. Also, in maghemite fine particles, Morales *et al.*[47] have reported a linear correlation between saturation magnetization and particle size, suggesting that defects at the particle surface can influence the magnetic properties.

The present results in Fe_3O_4 particles show that M_S at 5 K (where particles are blocked) does not scale with d^2 as expected if contributions from a magnetically disordered surface phase were present. Therefore, we also examined the possibility of the observed decrease in M_S being due to changes in *A*- and *B*-site population, which can change the resulting ferrimagnetic moment. These size effects on the inversion degree of several other spinel systems such as $ZnFe_2O_4$ and $CuFe_2O_4$ are well established[48–50] especially in Zn-ferrite, where large changes in M_S and T_C have been reported.[36,51] Using the notation $[Fe^{3+}]^A[Fe^{3+}Fe^{2+}]^BO_4$ for the ionic distribution, it can be easily calculated that even for a full inversion of Fe^{2+} ions from *B* to *A* sites, a maximum of ~20% of change in the net magnetic moment can be expected, which is only half of the ~40% observed between the M150 and M5 samples. Thus, this effect does not suffice to explain the observed decrease in M_S, and spin disorder at the surface and/or spin canting is also needed to explain this reduction.

Bulk magnetite is known to be magnetically soft, with values of coercive force $H_C\sim 200-400$ Oe at room temperature[34] that depends on the structural characteristics. For particles below a critical diameter D_S a single-domain behavior is expected. For a given temperature, H_C decreases from its maximum value $H_C(D_S)$ to zero with decreasing particle size due to the superparamagnetic relaxation effects. For the present samples, the onset of SPM relaxation takes place below $\langle d\rangle=10$ nm as inferred from the H_C values. At $T=5$ K, the remanence-to-saturation ratio $R=M_R/M_S$ for all samples studied (see Table I) are much smaller than the expected $R=0.5$ value for noninteracting, randomly oriented particles with uniaxial symmetry. Deviations from the noninteracting values are expected, and moreover these low R values reveal the existence of interparticle interactions of antiferromagnetic nature.[52]

At $T=5$ K all particles are blocked, and the magnetic moments will reverse by rotation. From the field-cooling procedure used in the present measurements, a full alignment of the individual particles should be expected. For Fe_3O_4 phase below T_V, the magnetocrystalline anisotropy is expected to be uniaxial, and the experimental coercivity field is related to the effective anisotropy constant K_{eff} through the relation $H_C=2K_{\text{eff}}/M_S$. From the above, valid for *noninteracting* particles with *uniaxial* anisotropy, we obtained $K_{\text{eff}}=3.9\times10^4$ erg/cm^3. This *effective value* obtained under the assumption of uniaxial anisotropy is clearly unphysical, since its magnitude is *below* the first-order magnetocrystalline anisotropy value $K_1^{\text{bulk}}=1.1-1.3\times10^5$ erg/cm^3 of bulk magnetite.[19,53] This result implies that the transition from cubic-to-uniaxial crystalline symmetry does not take place even at $T=5$ K, which is also supported by the absence of Verwey transition observed in $M(T)$ curves. We have, therefore, assumed the cubic anisotropy of the material to estimate the particle anisotropy, for which the anisotropy K_1 is related to the effective value by $K_{\text{eff}}=K_1/12$, provided that $K_1<0$.[54] For the present particles the above assumption yields $K_1=4.68\times10^5$ erg/cm^3, which is consistent with K_1^{bulk}, although increased by the dipolar contribution to the local field. It is interesting to compare these results with the value $K_{\text{eff}}=2.3\times10^4$ erg/cm^3 obtained by Luo *et al.*[40] in Fe_3O_4 particles with $d=5$ nm diluted in a frozen fluid, where dipolar interactions are much less important. This value yields $K_1=2.7\times10^5$ erg/cm^3, closer than our value to K_1^{bulk} but still larger. We have further checked our results using the same method of Ref. 40, based on the area within the hysteresis cycle, to estimate K_{eff}.[55] This method gives $K_{\text{eff}}=5.2\times10^4$ erg/cm^3, in reasonable agreement with results from coercive fields.

The existence of particle interactions makes the analysis of the *single-particle* magnetic anisotropy difficult to achieve, since contributions from the neighbor magnetic dipoles to the local field can be even larger than the intrinsic (crystalline or shape) anisotropy. The phenomenological expression generally used for describing the anisotropy K_{eff} of spherical particles of diameter d has been put forward by Bødker *et al.*,[56]

$$K_{\text{eff}} = K_V + \frac{6}{d} K_S , \tag{4}$$

where K_V is the bulk anisotropy energy per unit volume, and K_S is the surface density of anisotropy energy. From symmetry arguments, and assuming that surface anisotropy is normal to the particle surface, Bodker *et al.*[56] have demonstrated that a perfect spherical particle should have a zero net contribution from surface anisotropy. This argument was utilized in the same work to explain the value of K_S inferred for a system of spherical α-Fe nanoparticles, which was six orders of magnitude smaller than the surface anisotropy K_S measured for α-Fe thin films.[56,57] However, Eq. (4) does not take into account the existence of interparticle (e.g., dipolar) interactions, and therefore overestimates K_S (or K_{eff}) in concentrated systems. As shown from TEM pictures, the present Fe_3O_4 particles are nearly spherical, so no contribution from the surface should be expected. Consequently, the observed enhancement of the particle anisotropy should be mainly related to the effect of dipolar interactions rather than to a surface with larger anisotropy.

The large difference between values of K_{eff} obtained from static and dynamic measurements, 0.39 and 35.6 $\times 10^5$ erg/cm^3 respectively, can be explained qualitatively by considering the different magnetic regimes of each measurement. When the applied field is larger than a certain value H_0 that satisfies $\mu H_0 = k_B T_B$, where μ is the particle moment and k_B is the Boltzmann constant, it can be expected that the magnetic energy dominates the interaction energy. It has been demonstrated[40] that for weakly interacting Fe_3O_4 particles these two field regimes are separated by $H_0 \approx 150$ Oe, and for the high field regime the values of T_B do not depend on the particle interactions. In the present case, the higher concentration results in larger T_B values, and accordingly we calculated $H_0 \approx 460$ Oe. Therefore, the dynamic value of K_{eff}, obtained at $H \approx 0$, should be largely affected by the presence of dipolar interactions, whereas the static measure is essentially determined in the regime ($H = 70$ kOe) dominated by the external field.

Studies on thin-film saturation magnetization at room temperature showed a decrease of the magnetic moment at the interface, which was modeled with nonmagnetic or disordered, ''dead'' interface layers of 0.7 nm.[44] Depth-selective Mössbauer spectra measurements of 50.0- and 100-nm-thick bulk-like films indicated that the interface, surface, and bulk layers have the same magnetic properties, including the characteristic charge-ordering Verwey transition.[58] In a more recent work on ultrathin layers (thickness $\sim$5 nm),[15] it was also demonstrated that the properties of the surface and interface layers were not different from the interior, i.e., no dead layer existed on these films. Our results point to the latter picture, i.e., the particles have an intrinsic magnetic anisotropy similar to bulk value, although a spin disorder at the surface yields reduction of the magnetic moment.

In summary, we have studied the structural and magnetic properties of nearly spherical magnetite particles of different average sizes, showing the gradual evolution from bulk-like to single-domain behavior. Although spin disorder at the surface was needed to explain the reduction of the magnetic moment, no evidence was found of enhancement of the magnetic anisotropy at the surface, nor of exchange coupling between particle surface and core. We have found that the static and dynamic properties can be understood by considering changes in the single-particle anisotropy energy E_a through the effect of interparticle interactions in these concentrated systems.

ACKNOWLEDGMENTS

Three of the authors (T.S.B., F.C.F., and G.F.G.) are thankful to the Brazilian agencies FAPESP and CNPq for providing financial support.

[1] R. Gensler, P. Groppel, V. Muhrer, and N. Müller, Part. Part. Syst. Charact. **19**, 293 (2002).
[2] M. Salerno, J. R. Krenn, B. Lamprecht, G. Schider, H. Ditlbacher, N. Felidj, A. Leitner, and F. R. Aussenegg, Opto-Electron. Rev. **10**, 217 (2002).
[3] M. Todorovic, S. Schultz, J. Wong, and A. Scherer, Appl. Phys. Lett. **74**, 2516 (1999).
[4] M. Rutnakornpituk, M. S. Thompson, L. A. Harris, K. E. Framer, A. R. Esker, J. S. Riffle, J. Connolly, and T. G. St. Pierre, Polymer **43**, 2337 (2002).
[5] R. S. Molday and D. MacKenzie, J. Immunol. Methods **52**, 353 (1982).
[6] A. Jordan, R. Scholz, P. Wust, H. Schirra, T. Schiestel, H. Schmidt, and R. Felix, J. Magn. Magn. Mater. **194**, 185 (1999).
[7] K. F. Berggren and I. I. Yakimenko, Phys. Rev. B **66**, 085323 (2002).
[8] N. Sanz, P. L. Baldeck, and A. Ibañez, Synth. Met. **115**, 229 (2000).
[9] X. J. Zhang, S. A. Jenekhe, and J. Perlstein, Chem. Mater. **8**, 1571 (1996).
[10] X. Batlle and A. Labarta, J. Phys. D **35**, R15 (2002).
[11] P. Poddar, T. Fried, and G. Markovich, Phys. Rev. B **65**, 172405 (2002).
[12] H. Seo, M. Ogata, and H. Fukuyama, Phys. Rev. B **65**, 085107 (2002).
[13] S. P. Sena, R. A. Lindley, H. J. Blythe, C. H. Sauer, M. Al-Kafarji, and G. A. Gehring, J. Magn. Magn. Mater. **176**, 111 (1997).
[14] D. T. Margulies, F. T. Parker, F. E. Spada, R. S. Goldman, J. Li, R. Sinclair, and A. E. Berkowitz, Phys. Rev. B **53**, 9175 (1996).
[15] F. C. Voogt, T. T. M. Palstra, L. Niesen, O. C. Rogojanu, M. A. James, and T. Hibma, Phys. Rev. B **57**, R8107 (1998).
[16] T. Margulies, F. T. Parker, M. L. Rudee, F. E. Spada, J. N. Chapman, P. R. Aitchison, and A. E. Berkowitz, Phys. Rev. Lett. **79**, 5162 (1997).
[17] F. C. Voogt, T. Fujii, P. J. M. Smulders, L. Niesen, M. A. James, and T. Hibma, Phys. Rev. B **60**, 11193 (1999).
[18] T. Hibma, F. C. Voogt, L. Niesen, P. A. A. Van der Heijden, W. J. M. de Jonge, J. J. T. M. Donkers, and P. J. Vander Zaag, J. Appl. Phys. **85**, 5291 (1999).
[19] L. Bickford, Jr., J. Brownlow, and F. R. Penoyer, Proc. IEEE **104**, 238 (1957).
[20] C. Medrano, M. Schlenker, J. Baruchel, J. Espeso, and Y. Miyamoto, Phys. Rev. B **59**, 1185 (1999).
[21] M. P. Morales, T. González-Carreño, and C. J. Serna, J. Mater. Res. **7**, 2538 (1992).
[22] T. Sugimoto and E. Matijevic, J. Colloid Interface Sci. **74**, 227 (1980).
[23] R. Massart and V. Cabuil, J. Chem. Phys. **84**, 967 (1987).
[24] J. Lee, T. Isobe, and M. Senna, J. Colloid Interface Sci. **177**, 490 (1996).
[25] C. M. Sorensen, in *Nanoscale Materials in Chemistry*, edited by K. J. Klabunde (Wiley, New York, 2001), p. 169.
[26] C. Kittel, Phys. Rev. **70**, 965 (1946).
[27] Y. Miyamoto and S. J. Chikazumi, J. Phys. Soc. Jpn. **57**, 2040 (1988).
[28] R. S. Hargrove and W. Künding, Solid State Commun. **8**, 303 (1970).
[29] M. Sorescu, A. Grabias, R. A. Brand, J. Voss, D. Tarabasanu-Mihaila, and L. Diamandescu, J. Magn. Magn. Mater. **246**, 399 (2002).
[30] C. Caizer, J. Phys.: Condens. Matter **15**, 765 (2003).
[31] P. V. Hendriksen, S. Linderoth, and P. A. Lindgard, J. Phys.: Condens. Matter **5**, 5675 (1993).
[32] G. Xiao and C. L. Chien, J. Appl. Phys. **61**, 3308 (1987).
[33] B. Martínez, A. Roig, X. Obradors, E. Molins, A. Rouanet, and C. Monty, J. Appl. Phys. **79**, 2580 (1996).
[34] R. M. Cornell and U. Schwertmann, in *The Iron Oxides* (VCH, New York, 1996), Chaps. 2 and 6.

[35] J. L. Dormann, D. Fiorani, and E. Tronc, Adv. Chem. Phys. **XCVIII**, 326 (1997).
[36] G. F. Goya, IEEE Trans. Magn. **38**, 2610 (2002).
[37] J. A. De Toro, M. A. López de la Torre, M. A. Arranz, J. M. Riveiro, J. L. Marínez, P. Palade, and G. Filoti, Phys. Rev. B **64**, 094438 (2001).
[38] F. Luis, F. Petroff, J. M. Torres, L. M. García, J. Bartolomé, J. Carrey, and A. Vaurès, Phys. Rev. Lett. **88**, 217205 (2002).
[39] G. F. Goya, F. C. Fonseca, R. F. Jardim, R. Muccillo, N. L. V. Carreño, E. Longo, and E. R. Leite, J. Appl. Phys. **93**, 6531 (2003).
[40] W. Luo, S. R. Nagel, T. F. Rosenbaum, and R. E. Rosensweig, Phys. Rev. Lett. **67**, 2721 (1991).
[41] T. Kendelewicz, P. Liu, C. S. Doyle, G. E. Brown, Jr., E. J. Nelson, and S. A. Chambers, Surf. Sci. **453**, 32 (2000).
[42] T. Sato, T. Iijima, M. Sekin, and N. Inagaki, J. Magn. Magn. Mater. **65**, 252 (1987).
[43] W. F. J. Fontijn, *et al.*, J. Magn. Magn. Mater. **165**, 401 (1997).
[44] P. A. A. van der Heijden, P. J. H. Bloemen, J. M. Gaines, J. T. W. M. van Eemeren, R. M. Wolf, P. J. van der Zaag, and W. J. M. de Jonge, J. Magn. Magn. Mater. **159**, L293 (1996).
[45] S. Chikazumi, *Physics of Magnetism* (Wiley, New York, 1964), p. 100.
[46] J. M. D. Coey, Phys. Rev. Lett. **27**, 1140 (1971).
[47] M. P. Morales, M. Andres-Verges, S. Veintemillas-Verdaguer, M. I. Montero, and C. J. Serna, J. Magn. Magn. Mater. **203**, 146 (1999).
[48] J. Z. Jiang, G. F. Goya, and H. R. Rechenberg, J. Phys.: Condens. Matter **11**, 4063 (1999).
[49] G. F. Goya and H. R. Rechenberg, J. Magn. Magn. Mater. **203**, 141 (1999).
[50] G. F. Goya, H. R. Rechenberg, and J. Z. Jiang, J. Magn. Magn. Mater. **218**, 221 (2000).
[51] G. F. Goya and H. R. Rechenberg, J. Magn. Magn. Mater. **196-197**, 191 (1999).
[52] G. Hadjipanayis, D. J. Sellmyer, and B. Brandt, Phys. Rev. B **23**, 3349 (1981).
[53] B. D. Cullity, in *Introduction to Magnetic Materials* (Addison-Wesley, Reading, MA, 1972), p. 234.
[54] J. I. Gittleman, B. Abeles, and S. Bozowski, Phys. Rev. B **9**, 3891 (1974).
[55] J. J. Prejean and M. J. Joliclerc, J. Phys. (Paris) **41**, 427 (1980).
[56] F. Bodker, S. Mørup, and S. Linderoth, Phys. Rev. Lett. **72**, 282 (1994).
[57] K. B. Urquhart, B. Heinrich, J. F. Cochran, A. S. Arrott, and K. Myrtle, J. Appl. Phys. **64**, 5334 (1988).
[58] T. Fujii, M. Takano, R. Katano, Y. Isozumi, and Y. Bando, J. Magn. Magn. Mater. **130**, 267 (1994).